

REFERENCES

- Adamson, A.W. (1990) Physical Chemistry of Surfaces. New York: John Wiley & Sons.
- Chatelier, R.C., Hodges, A.M., Drummond, C.J., Chan, D.Y., and Griesser, H.J. (1997) Determination of the intrinsic acid-base dissociation constant and site density of ionizable surface groups by capillary rise measurements. Langmuir, 13, 3043-3046.
- Fennell E., D. and Wennerstrom H., I.(1994) The Colloidal Domain where Physics, Chemistry, Biology, and Technology Meet. USA: VCH Publishers, Inc.
- Fox, R.W. and McDonald, A.T. (1994) Introduction to Fluid Mechanics. 4th ed. USA: John Wiley & Sons.
- Grzybowski, B.A., Arias, F., Yang H., and Whitesides, G.M. (2001) Modeling of menisci and capillary forces from the millimeter to the micrometer size range. Journal of Physics and Chemistry B, 105, 404-412.
- Hahn, J. and Sibener, S.J. (2000) Cylinder alignment in annular structures of microphase-separated polystyrene-b-poly(methyl methacrylate). Langmuir, 16, 4766-4769.
- Holman, J.P.(1997) Heat Transfer. 8th ed., USA: McGraw-Hill, Inc.
- Hunter, R.J.(1986) Foundations of Colloid Science Volume I. New York: Oxford University Press.
- Lee, S., Kim, D.H., and Needham, D. (2001) Equilibrium and dynamic interfacial tension measurements at microscopic interfaces using a micropipet technique. 1.A new method for determination of interfacial tension. Langmuir, 17, 5537-5543.
- Neumann, A.W. and Spelt, J. K. (1996) Applied Surface Thermodynamics. Surfactant Science Series. Vol. 63, New York: Marcel Dekker.
- Middleman, S. (1998) An Introduction to Fluid Dynamics: Principles of Analysis and Design. USA: John Wiley & Sons.
- Miller C.A. and Neogi, P. (1985) Interfacial phenomena: equilibrium and dynamic effects, Surfactant Science Series. 17, pp.23-41. New York: Marcel Dekker.

- Morrison, Iran D. (2002) Colloidal Dispersions: Suspensions, Emulsions, and Foams. USA: John Wiley & Sons.
- Paul Hiemenz, C. (1986) Principles of Colloid and Surface Chemistry. Vol.9, New York: Marcel Dekker, Inc.
- Piron, D.L.(1991) The Electrochemistry of Corrosion. USA: National Association of Corrosion Engineers.
- Raymond Canale, P. and Steven Chapra, C. (2003) Numerical Methods for Engineers. 4th ed., Singapore: McGraw-Hill.
- Rosen, M.J. (1989) Surfactant and Interfacial Phenomena. 2nd ed., USA: John Wiley & Sons.
- Ruijter, M. D., Kolsch, P., Voue, M., Coninck, J. D., and Rabe, J.P. (1998) Effect of temperature on the dynamic contact angle. Colloids and Surfaces A: Physicochemical and Engineering Aspects, 44, 235-243.
- Wilkes James, O.(1999) Fluid Mechanics for Chemical Engineers. New Jersey: Prentice-Hall, Inc.
- Nakamatsu, J.K., Delgado-Aparicio, L.F.V., Da Silva A., and Soberon, F.V. P. (2000) Ageing of Plasma-Treated Polytetrafluoroethylene Surfaces. http://www.pucp.edu.pe/~gip/articles/articulo_ageing.doc

APPENDICES

Appendix A Numerical solution of differential equations by Euler's method.

Here, the sample of mathematical model is presented by means of the numerical technique which can readily be adapted to the solution of more complicated problems, differential equations.

Consider the following differential equation, which occurred (with differential notation) in the prophecy of meniscus characteristic in the section 3.1.2, circular annulus surface:

$$\frac{1}{R_1} + \frac{1}{R_2} = \frac{\frac{d^2 h}{dr^2}}{\left[1 + \left(\frac{dh}{dr}\right)^2\right]^{3/2}} + \frac{\frac{dh}{dr}}{r \left[1 + \left(\frac{dh}{dr}\right)^2\right]^{1/2}} \quad (\text{A.1})$$

Since the Equation (A.1) is the second-order nonlinear differential equation. Therefore, it is changed to the first-order differential equation by assuming

$$\phi = \frac{dh}{dr} \quad (\text{A.2})$$

The first-order differential equation, which is adjusted, can be simply solved with correlation of

$$\frac{d\phi}{dr} = f(\phi, r) \quad (\text{A.3})$$

where $f(\phi, r)$ is the differential equation evaluated at ϕ and r , while the estimation is managed by Euler's method below

$$\phi_{i+1} = \phi_i + \frac{d\phi}{dr}(\Delta r) \quad (\text{A.4})$$

In this even, the slope estimate of $d\phi/dr$ is used to extrapolate from an old value ϕ_i to a new value ϕ_{i+1} over a step size Δr .

After that, the ordinary differential equation is again solved by the form of

$$\frac{dh}{dr} = f(h, r) \quad (\text{A.5})$$

where $f(h, r)$ is the differential equation evaluated at h and r , as the evaluation can be done along the way of

$$h_{i+1} = h_i + \phi(\Delta r) \quad (\text{A.6})$$

The values h_i and h_{i+1} are the dependent variables at the beginning and end of the i th step size, of duration Δr .

Meniscus attribute is predicted starting from the meniscus tip location up to where the meniscus surface touched with the annular tube wall. In this regard, we can know the parameters at the beginning of estimation, the meniscus tip, there are

$$\phi = \frac{dh}{dr} = h = 0 \quad \text{at } r = 0 \quad (\text{A.7})$$

On the other hand, the point of meniscus surface contacted with the annular tube wall also present the parameter at the end of estimation, there are

$$\frac{dh}{dr} = \cot \theta \quad \text{at } r = \text{Gap width} / 2 \quad (\text{A.8})$$

Then, the problem is untangled by the repetitive nature of the calculations. Euler's method is readily implemented via spreadsheet, as demonstrably shown in Table A.1

The spreadsheet of Euler's method solving problem in Table A.1 is for study of water rise inside the vertical annular tube at inner/outer tube of 7/10 mm with circular annulus assumption, where

$$\phi = \frac{dh}{dr} = h = 0 \quad \text{at } r = 0$$

and

$$\frac{dh}{dr} = \cot 10^\circ \quad \text{at } r = 0.5/2 = 0.25$$

Table A.1 Spreadsheet implementation of Euler's method with circular annulus surface for meniscus in vertical annular tube of 7/10 mm

	A	B	C	D	E	F	G
	R(mm)	h(mm)	dh/dr	ϕ	d ϕ /dr(1/mm)	R ₁ =R ₂ =R(mm)	H(mm)
1	0	0	0	0	3.94336596	0.126795231	28.9373
2	0.0001	0	0.00039	0.00039	3.94336688		
3	0.0002	3.94E-08	0.00078	0.00078	3.94336964		
4	0.0003	1.18E-07	0.00118	0.00118	3.94337424		
5	0.0004	2.37E-07	0.00157	0.00157	3.94338067		
6	0.0005	3.94E-07	0.00197	0.00197	3.94338895		
7	0.0006	5.92E-07	0.00236	0.00236	3.94339907		
8	0.0007	8.28E-07	0.00276	0.00276	3.94341103		
9	0.0008	1.1E-06	0.00315	0.00315	3.94342483		
10	0.0009	1.42E-06	0.00354	0.00354	3.94344046		
11	0.0010	1.77E-06	0.00394	0.00394	3.94345794		
12	0.0011	2.17E-06	0.00433	0.00433	3.94347726		
13	0.0012	2.6E-06	0.00473	0.00473	3.94349841		
14	0.0013	3.08E-06	0.00512	0.00512	3.94352141		
15	0.0014	3.59E-06	0.00552	0.00552	3.94354624		
16	0.0015	4.14E-06	0.00591	0.00591	3.94357292		
2502	0.2500	0.209877	5.6715	5.6715	753.729939		

Relating to this spreadsheet, observe the following:

1. Digits and letters identify the various rows and columns.
2. In row 1, all of the parameters at the beginning of estimation are entered into the cells such as $r = 0$ in cell A1, $h = 0$ in cell B1, $dh/dr = \phi = 0$ in both cells C1 and D1.
3. In column E onwards, the formula of Equation (A.1) is entered into cells and causes the indicated numerical values to appear.
4. Once Euler's procedures in the Equations (A.4) and (A.6) have been entered, such as that in cell D2 and B2, respectively. They can be "pasted" into subsequent cells in its column; the row counter will thereby be incremented automatically.
5. Dollar signs indicate an absolute cell address, which will not change when a formula is pasted into subsequent cells.

6. The expression of $(=A1+0.0001)$ is got in cell A2 and then paste that expression from cell A2 into subsequent cells in column A, while the value 0.0001 is intensive and appropriated step size which has generated answers that are surprisingly excellent. If required, the extreme accuracy could easily be improved by taking a smaller step size (and performing more calculations).
7. The correlation between the curvature of the surface and the height of liquid rise in annular tube is also put into cell F1, that is $R = \gamma / \rho gh$, as follow Equation (3.19).
8. The parameter H, the height of liquid rise in annular tube, is not built into any of the formulas, but are located to its own cell in G1. The trial and error is needed to guess the exactly right value of H that can propose dh/dr in cell C2502, the end of estimation at $r = 0.25$, equals to $\cot 10^\circ$ or 5.6715.

Appendix B Demonstration of the pictures of water rise inside annular tube for experiments.

The experiments were done according to the instruction in chapter IV, meanwhile the photographs of water rise in annular tube performed by those experiments are illustrated in this section.

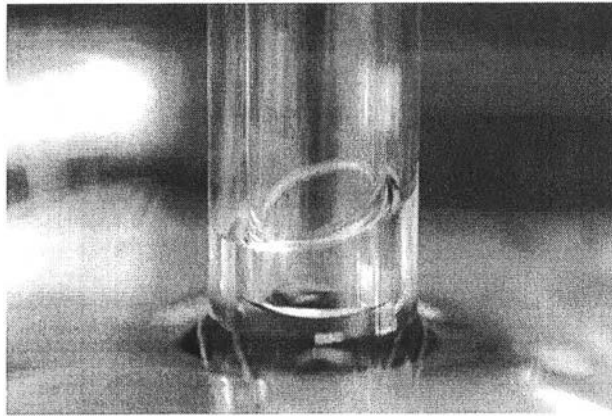


Figure B.1 The unequal rise of water during the vertical annular tube experiment.

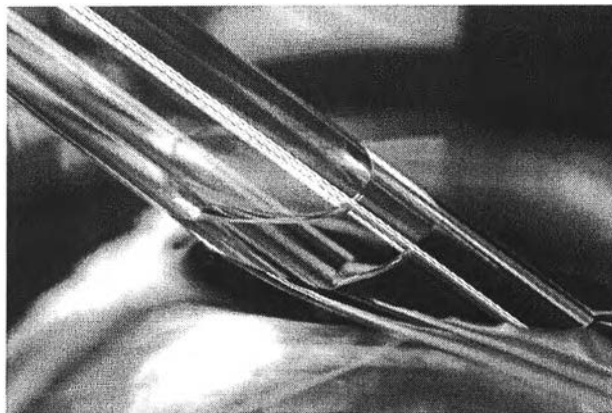


Figure B.2 The water rise in inclined annular tube at 30° inclination.

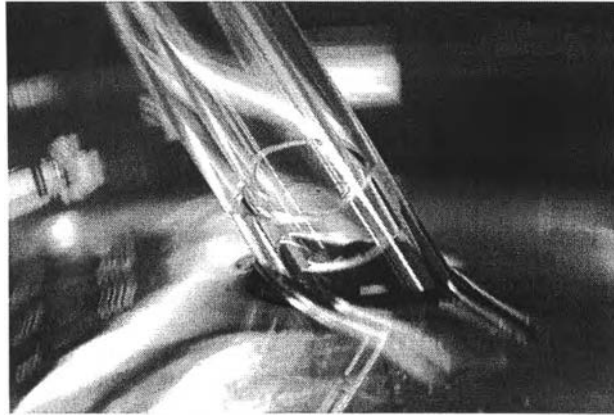


Figure B.3 The water rise in inclined annular tube at 45° inclination.

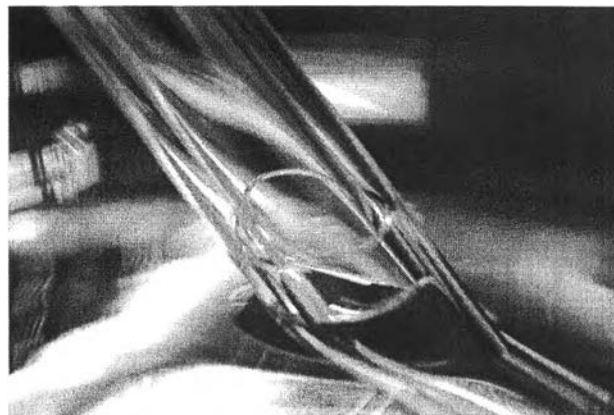


Figure B.4 The water rise in inclined annular tube at 60° inclination.



Figure B.5 The water rise in annular cone at 45° opening angle.

Appendix C Mathematical calculation by using Force-Balance analysis.

This section was proposed to examine the model by using the relation of gravitational force and surface tension force.

The mass M of an object is a measure of the amount of matter. On the other hand, the weight w of the object is the gravitational force on it, and is equal to Mg , where g is the local gravitational acceleration.

The surface tension force operates along the entire meniscus edge, varies linearly with the length l of the meniscus, and is equal to $\gamma 2 \pi r$.

At equilibrium, these two forces are equated, giving

$$\text{gravitational force} = \text{surface tension force}$$

C.1 Vertical Annular Tube

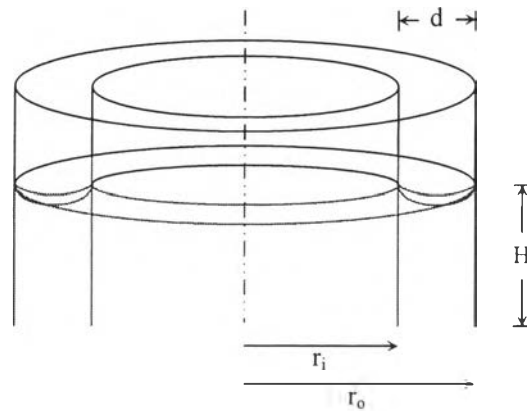


Figure C.1 The schematic diagram of the capillary rise in vertical annular tube.

$$\text{gravitational force} = \text{surface tension force}$$

$$Mg = \gamma l$$

$$\rho g (\pi r_o^2 - \pi r_i^2) H = \gamma (2 \pi r_o + 2 \pi r_i) \cos \theta_i$$

$$\rho g \pi (r_o^2 - r_i^2) H = 2 \pi \gamma (r_o + r_i) \cos \theta_i$$

$$\rho g \pi (r_o - r_i)(r_o + r_i) H = 2 \pi \gamma (r_o + r_i) \cos \theta_i$$

$$\begin{aligned}
 H &= \frac{2\gamma \cos \theta_i}{\rho g(r_o - r_i)} \\
 H &= \frac{2\gamma \cos \theta_i}{\rho g d} \quad (C.1)
 \end{aligned}$$

C.2 Inclined Annular Tube

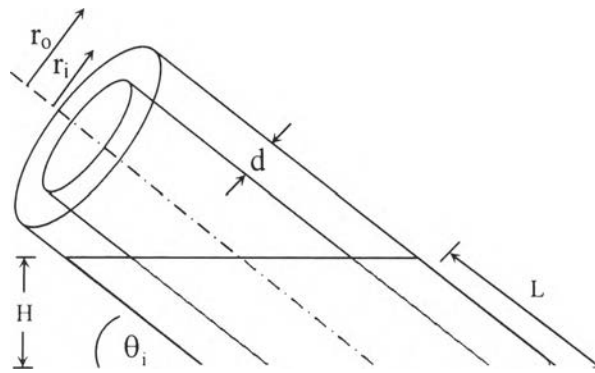


Figure C.2 The schematic diagram of the capillary rise in inclined annular tube.

gravitational force = surface tension force

$$Mg = \gamma l$$

$$\begin{aligned}
 \rho g(\pi r_o^2 - \pi r_i^2)L &= \frac{1}{2} \left[\left(\gamma 2\pi r_o \cos(90^\circ - \theta_i + \theta) + \gamma 2\pi r_o \cos(90^\circ - \theta_i - \theta) \right) + \right. \\
 &\quad \left. \left(\gamma 2\pi r_i \cos(90^\circ - \theta_i + \theta) + \gamma 2\pi r_i \cos(90^\circ - \theta_i - \theta) \right) \right]
 \end{aligned}$$

$$\begin{aligned}
 \rho g(\pi r_o^2 - \pi r_i^2) \frac{H}{\sin \theta_i} &= \gamma \pi \left[\left(r_o \cos(90^\circ - \theta_i + \theta) + r_o \cos(90^\circ - \theta_i - \theta) \right) + \right. \\
 &\quad \left. \left(r_i \cos(90^\circ - \theta_i + \theta) + r_i \cos(90^\circ - \theta_i - \theta) \right) \right]
 \end{aligned}$$

$$\begin{aligned}
 H &= \left\{ \gamma \pi \sin \theta_i \left[\left(r_o \cos(90^\circ - \theta_i + \theta) + r_o \cos(90^\circ - \theta_i - \theta) \right) + \right. \right. \\
 &\quad \left. \left. \left(r_i \cos(90^\circ - \theta_i + \theta) + r_i \cos(90^\circ - \theta_i - \theta) \right) \right] \right\} / \rho g(\pi r_o^2 - \pi r_i^2)
 \end{aligned}$$

$$\begin{aligned}
 H &= \left\{ \gamma \sin \theta_i \left[\left(r_o \cos(90^\circ - \theta_i + \theta) + r_o \cos(90^\circ - \theta_i - \theta) \right) + \right. \right. \\
 &\quad \left. \left. \left(r_i \cos(90^\circ - \theta_i + \theta) + r_i \cos(90^\circ - \theta_i - \theta) \right) \right] \right\} / \rho g(r_o^2 - r_i^2) \quad (C.2)
 \end{aligned}$$

C.3 Annular Cone

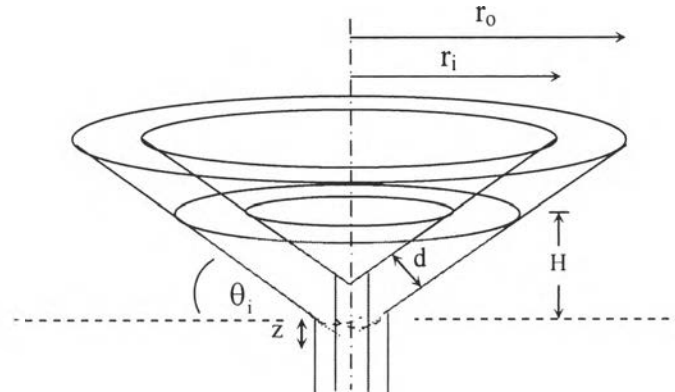


Figure C.3 The schematic diagram of the capillary rise in annular cone.

From Figure C.3, we obtain

$$\begin{aligned}\cos \theta_i &= \frac{d}{z} \\ z &= \frac{d}{\cos \theta_i}\end{aligned}\quad (C.3)$$

and

$$\begin{aligned}\tan \theta_i &= \frac{H}{r} \\ r &= \frac{H}{\tan \theta_i}\end{aligned}\quad (C.4)$$

gravitational force = surface tension force

$$Mg = \gamma l$$

$$\begin{aligned}\rho g \left(\frac{1}{3} \pi r_o^2 (H+z) - \frac{1}{3} \pi r_i^2 H - \frac{1}{3} \pi (r_o-r_i)^2 z \right) &= \left(\gamma 2 \pi r_o \cos(90^\circ - \theta_i + \theta) \right) + \\ &\left(\gamma 2 \pi r_i \cos(90^\circ - \theta_i - \theta) \right)\end{aligned}$$

$$\frac{1}{3} \pi \rho g (r_o^2(H+z) - r_i^2H - (r_o-r_i)^2z) = 2\gamma \pi [(r_o \cos(90^\circ - \theta_i + \theta)) + (r_i \cos(90^\circ - \theta_i - \theta))]$$

$$\frac{1}{3} \rho g (r_o^2H + r_o^2z - r_i^2H - (r_o-r_i)^2z) = 2\gamma [(r_o \cos(90^\circ - \theta_i + \theta)) + (r_i \cos(90^\circ - \theta_i - \theta))]$$

Dealing with Equations (c.3) and (c.4), we are able to diminish r and z terms that is

$$\frac{1}{3} \rho g \left[\frac{(H+d/\cos\theta_i)^2}{\tan^2\theta_i} H + \frac{(H+d/\cos\theta_i)d}{\tan^2\theta_i \cos\theta_i} - \frac{H^3}{\tan^2\theta_i} - \left(\frac{H+d/\cos\theta_i}{\tan\theta_i} - \frac{H}{\tan\theta_i} \right)^2 d/\cos\theta_i \right] = 2\gamma \left[\left(\frac{H+(d/\cos\theta_i)}{\tan\theta_i} \cos(90^\circ - \theta_i + \theta) \right) + \left(\frac{H}{\tan\theta_i} \cos(90^\circ - \theta_i - \theta) \right) \right]$$

$$\frac{\rho g}{3 \tan^2\theta_i} \left[(H+(d/\cos\theta_i))^2 H + \frac{(H+d/\cos\theta_i)d}{\cos\theta_i} - H^3 - (d/\cos\theta_i)^3 \right] = \frac{2\gamma}{\tan\theta_i} \left[\left((H+d/\cos\theta_i) \cos(90^\circ - \theta_i + \theta) \right) + \left(H \cos(90^\circ - \theta_i - \theta) \right) \right]$$

$$\frac{\rho g}{3 \tan\theta_i} \left[(H+(d/\cos\theta_i))^2 H + \frac{(H+d/\cos\theta_i)d}{\cos\theta_i} - H^3 - (d/\cos\theta_i)^3 \right] = 2\gamma \left[\left((H+d/\cos\theta_i) \cos(90^\circ - \theta_i + \theta) \right) + \left(H \cos(90^\circ - \theta_i - \theta) \right) \right] \quad (C.5)$$

Appendix D Appearance of the radii of curvature on the curved surface under the water rising in annular tube.

The expression of radii of curvature R_2 is much greater than radii of curvature R_1 in case of water rising in annular geometry, was also explained in this section.

The radii of curvature R_1 and R_2 were designated over the water surface, while their characteristics were shown in the Figure D.1.

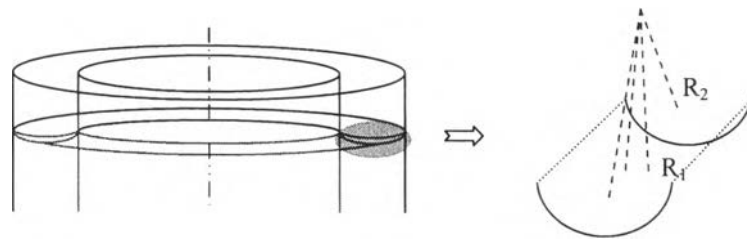


Figure D.1 The picture to show the radii of curvature on the water surface within annular geometry.

From the Equation (3.6), the local curvature can be approximated, that is

$$\frac{1}{R_1} + \frac{1}{R_2} = \frac{\frac{d^2h}{dr^2}}{\left[1 + \left(\frac{dh}{dr}\right)^2\right]^{3/2}} + \frac{\frac{dh}{dr}}{r \left[1 + \left(\frac{dh}{dr}\right)^2\right]^{1/2}}$$

The following expressions from analytical geometry is a general function for R_1^{-1} and R_2^{-1} on the surface, there are

$$R_1^{-1} = \frac{d^2h / dr^2}{\left[1 + (dh / dr)^2\right]^{3/2}} \quad (D.1)$$

and

$$R_2^{-1} = \frac{dh / dr}{r \left[1 + (dh / dr)^2\right]^{1/2}} \quad (D.2)$$

Applying a numerical method with shooting method solving both Equations (D.1) and (D.2). Then, the dimension of radii of curvature R_1 and R_2 can be

perceived and were presented in Table D.1, which are the radii of curvature results on the water surface in vertical annular tube alignment (fundamental results of annular geometry study).

Table D.1 The radii of curvature results on the water surface in vertical annular tube alignment

Inner/Outer Tube Diameter (mm)	R₁ (mm)	R₂ (mm)	1/R₁ (1/mm)	1/R₂ (1/mm)
7/10	0.2536	5.3411	3.9447	0.1872
10/15	0.7613	8.4283	1.3135	0.1186
15/20	0.7613	9.8290	1.3135	0.1017

Appendix E Comparison of meniscus configuration from modeling and experiment.

The annular tube consists of two capillary tubes; outer and inner capillary tubes. There are two menisci occurring; one in the inner capillary tube and the other in annulus. However, the clear picture of meniscus rising in annular tube could not be photographed. Therefore, the pictures of meniscus in inner capillary tube were used to compare with the meniscus in annular tube predicted by the model.



Figure E.1 Comparison of meniscus resulted from the model and experiment for vertical annular tube at inner/outer tube of 7/10 mm.



Figure E.2 Comparison of meniscus resulted from the model and experiment for vertical annular tube at inner/outer tube of 10/15 and 15/20 mm.

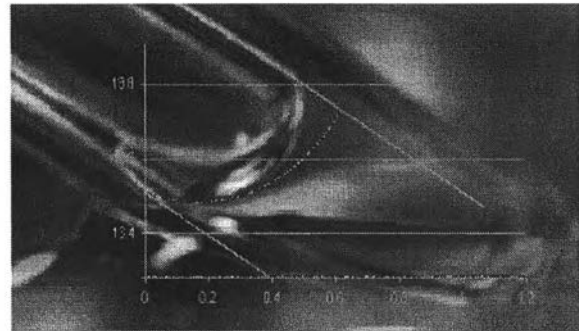
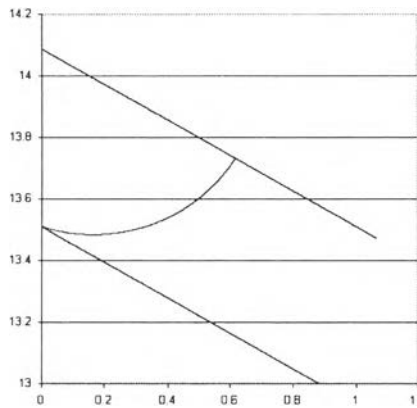


Figure E.3 Comparison of meniscus resulted from the model and experiment for inclined annular tube at inner/outer tube of 7/10 mm with 30° inclination.

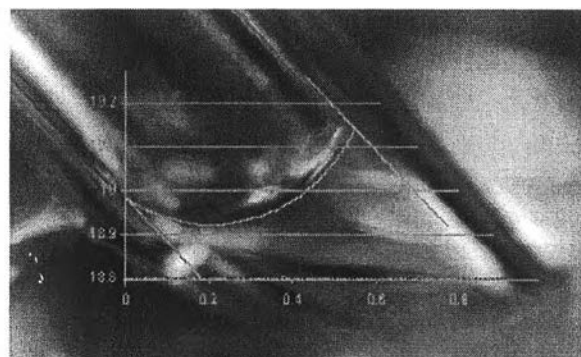
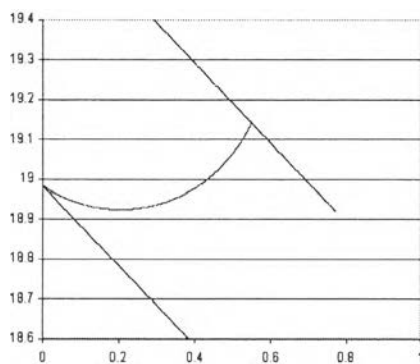


Figure E.4 Comparison of meniscus resulted from the model and experiment for inclined annular tube at inner/outer tube of 7/10 mm with 45° inclination.

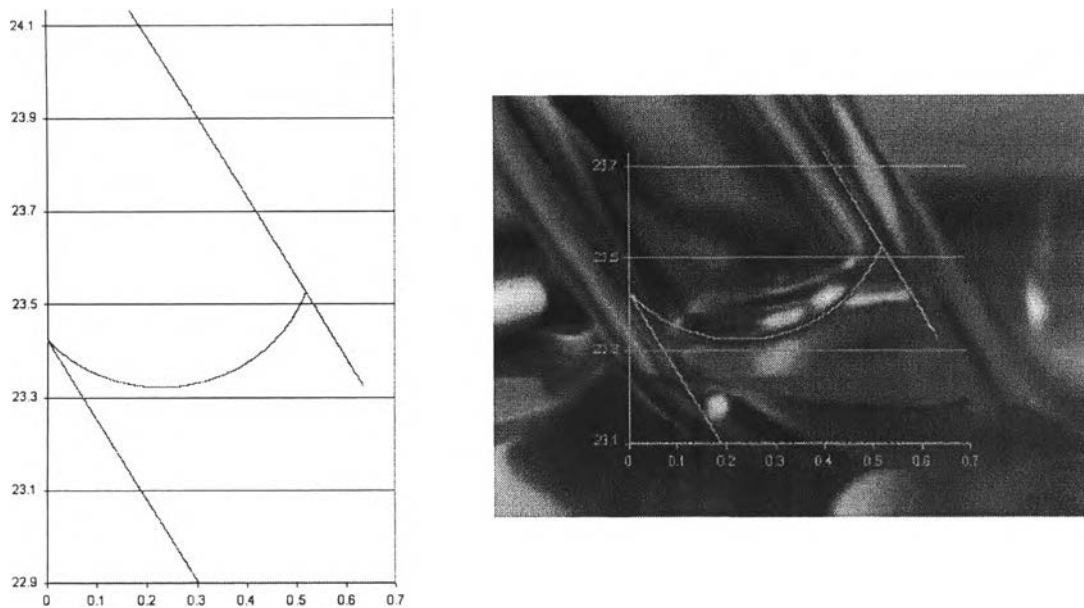


Figure E.5 Comparison of meniscus resulted from the model and experiment for inclined annular tube at inner/outer tube of 7/10 mm with 60° inclination.

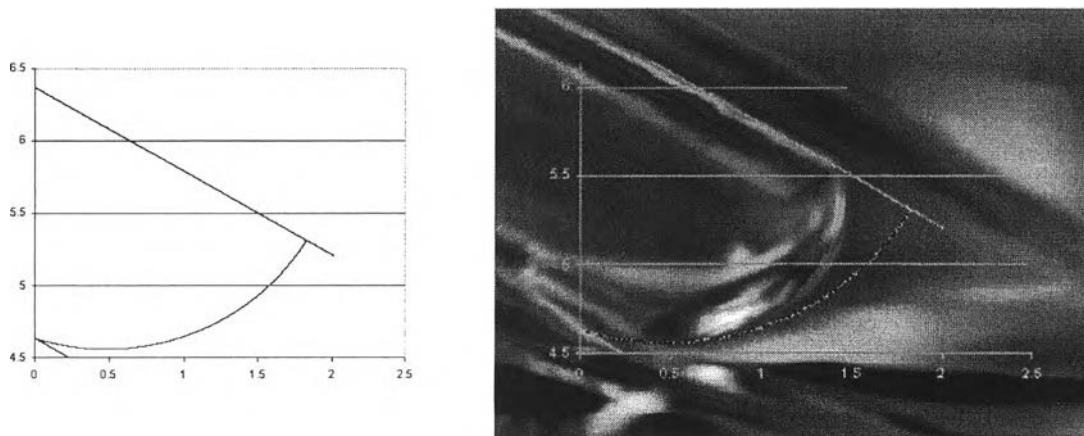


Figure E.6 Comparison of meniscus resulted from the model and experiment for inclined annular tube at inner/outer tube of 10/15 and 15/20 mm with 30° inclination.

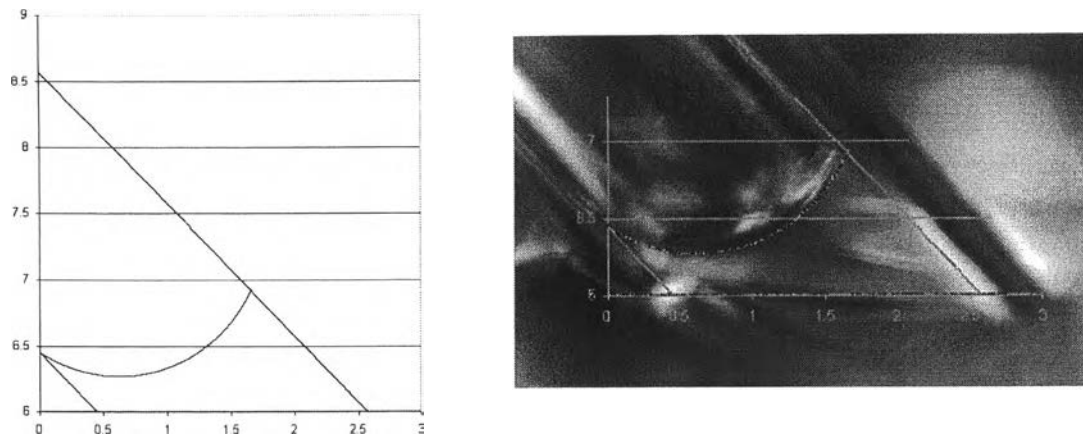


Figure E.7 Comparison of meniscus resulted from the model and experiment for inclined annular tube at inner/outer tube of 10/15 and 15/20 mm with 45° inclination.

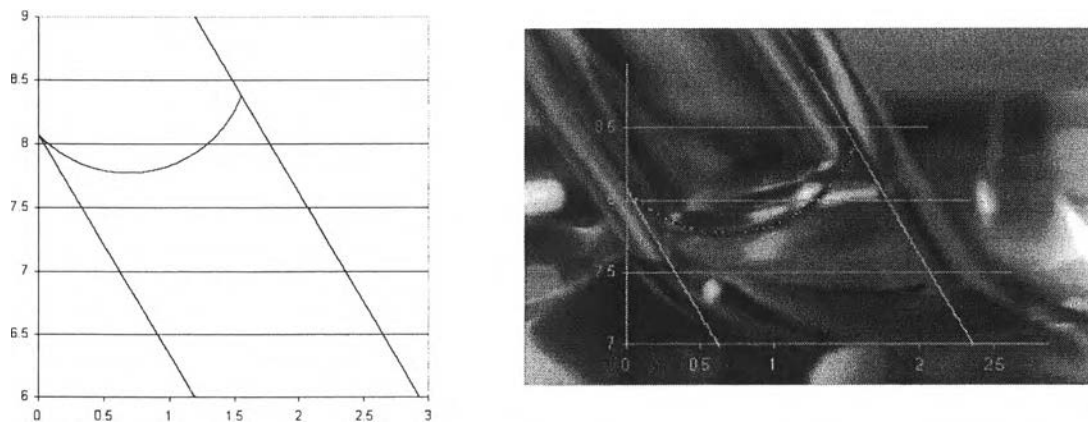


Figure E.8 Comparison of meniscus resulted from the model and experiment for inclined annular tube at inner/outer tube of 10/15 and 15/20 mm with 60° inclination.

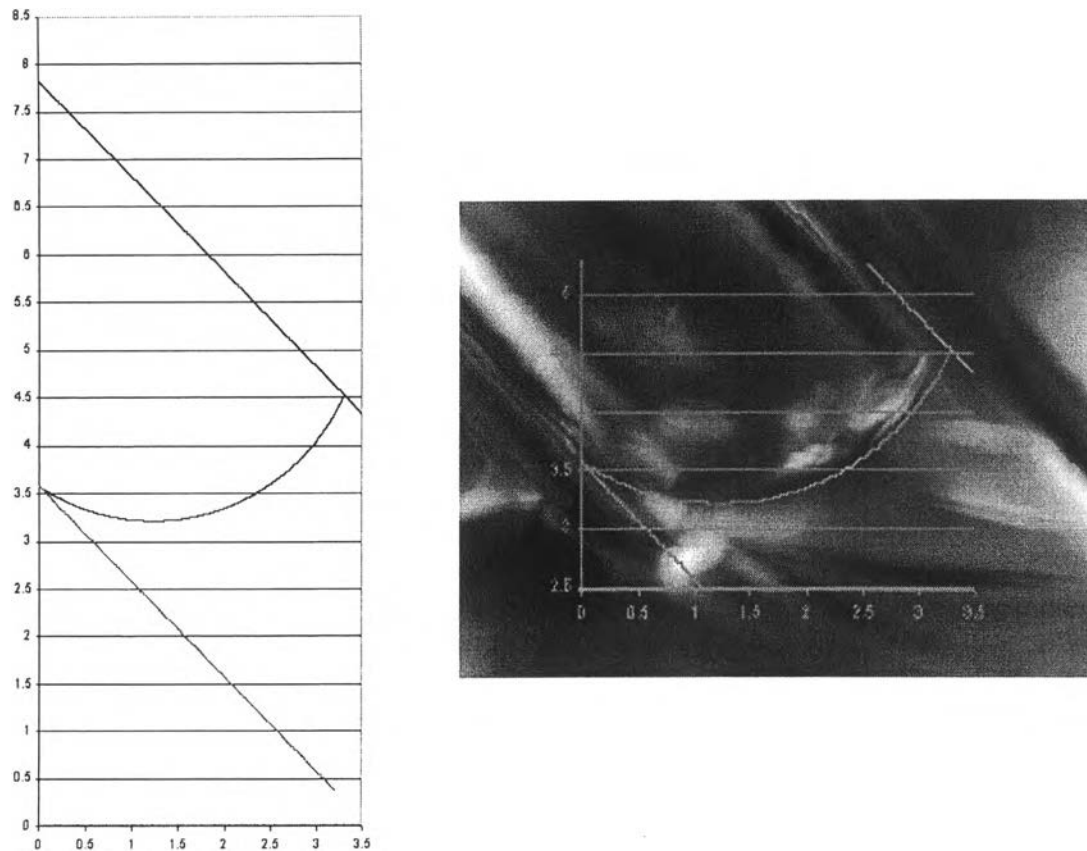


Figure E.9 Comparison of meniscus resulted from the model and experiment for annular cone at gap width 3.0 mm with 45° opening angle.

CURRICULUM VITAE

Name: Mr. Akekachai Nonpassopon

Date of Birth: July 11, 1980

Nationality: Thai

University Education:

1998-2002 Bachelor Degree of Chemical Engineering, Faculty of Engineering, King Mongkut Institute of Technology North Bangkok, Bangkok, Thailand.